

Check for updates

Additive-Regulated Interface Chemistry Enables Depolarization for Ultra-High Capacity LiCoO₂

Guorui Zheng,* Hengyu Ren, Jimin Qiu, Haowen Ding, Likun Chen, Yuhang Li, Shunning Li, Ming Liu,* and Feng Pan*

Unlocking the capacity potential of mainstream LiCoO2 (LCO) cathode materials for stable cycling at a high upper cut-off voltage is undoubtedly one of the most economical approaches to achieving high-energy-density lithium-ion batteries. However, significant polarization issues induced by interfacial and interphase degradation during high-voltage cycling remain well known. This study demonstrates the efficient depolarization effects of cyclic organosiloxane additive 2,4,6,8-tetramethyl-2,4,6,8-tetravinylcyclotetrasiloxane (V4D4) at the cathode-electrolyte interface, facilitating interfacial charge transfer and enhancing the capacity of LCO||Li cells to 220 mA h g^{-1} even at 4.55 V (vs Li/Li⁺). Specifically, V4D4 tends to adsorb onto the surface of highly delithiated LCO cathodes, and its preferential oxidation intermediates help stabilize lattice oxygen, eliminate harmful HF/H2O, and form an ultrathin cathode-electrolyte interphase (CEI) that reduces interface resistance to Li⁺ diffusion and stabilizes the surface structure. Additionally, with the assistance of fluoroethylene carbonate (FEC), long-term cycling produces a homogeneous, chemo-mechanically stable CEI enriched in organic silicon-containing compounds and LiF. This CEI suppresses excessive bulk electrolyte decomposition, reinforces the reversibility of the significantly enhanced O3-H1-3 phase transition, and enables capacity retention of ≈97% after 200 cycles.

1. Introduction

The actual capacity delivery of mainstream LiCoO $_2$ (LCO) cathode materials remains far below their theoretical specific capacity (\approx 274 mA h g $^{-1}$). Breaking through their upper limit at a cut-off voltage above 4.4 V (vs Li/Li $^+$, V $_{\rm Li}$) with further unlocking capacity potential for stable cycling is undoubtedly one of the

G. Zheng, H. Ren, J. Qiu, H. Ding, S. Li, F. Pan School of Advanced Materials

Peking University Shenzhen Graduate School

Shenzhen 518055, P. R. China

E-mail: zhengguorui@sz.tsinghua.edu.cn; panfeng@pkusz.edu.cn

G. Zheng, L. Chen, Y. Li, M. Liu Institute of Materials Research (IMR) Tsinghua Shenzhen International Graduate School Tsinghua University

Shenzhen 5 18055, P. R. China E-mail: liuming@sz.tsinghua.edu.cn

The ORCID identification number(s) for the author(s) of this article can be found under https://doi.org/10.1002/adma.202504106

DOI: 10.1002/adma.202504106

most economical approaches to achieving high-energy-density lithium batteries with strong potential for commercialization. [1,2] However, high-voltage (HV) cycling accelerates interfacial and interphase degradation, leading to significant polarization, limited capacity enhancement, and ultimately limited improvements in energy and power density, thereby deteriorating battery performance. [3,4]

For the unmodified LCO cathode subjected to a deep delithiation potential exceeding 4.55 V_{Li}, a series of unfavorable phase transitions from O3 to H1-3 or even O1 occur, involving large-scale sliding of O-Co-O slabs. These transitions promote lattice distortion, Li rearrangement, and volume shrinkage along the c-axis, which in turn cause partial structural collapse and heterogeneous delithiation.[5-7] Critically, a high-potential driving force and the generation of strongly oxidative Co^{4+}/O^{n-} (0<n<2) species induce severe interfacial side reactions, including excessive electrochemical catalytic decomposition of the electrolyte, loss of lattice O, and dissolution of lowvalence-state Co.[8] These effects can cause

irreversible Co migration and the formation of a dense Co₃O₄/CoO phase on the surface, which impedes Li⁺ diffusion and increases surface polarization, thereby leading to the propagation of collapse and cracks into the bulk particle structure, resulting in a rapid capacity loss as cycling progresses.^[9–11]

Therefore, to mitigate the adverse effects of inevitable phase transitions while targeting higher capacity delivery, constructing stable interfaces and interphases on the LCO cathode surface to prevent rapid deterioration spread to the bulk structure is essential.[12] Among available strategies, electrolyte-involved interfacial engineering is cost-effective and straightforward to implement in large-scale industrial production. However, several modification studies have limited their focus on increasing the charging cut-off voltage, which actually compromises part of the ineffective polarization potential, reduces energy conversion efficiency, and suppresses the so-called unfavorable O3—H1-3/O1 phase transitions, an inevitable process for achieving high capacity, ultimately limiting actual energy density enhancement and sacrificing cyclability and safety at extremely high charging voltages. Therefore, identifying a more efficient method requires focusing on regulating surface and interfacial stability

1521495, 2025, 44, Downloaded from https://dvanced online library.wiley.com/doi/10.1002adma.02504106 by University Town Of Shenzhen, Wiley Online Library on [1711/1025]. See the Terms and Conditions (https://onlinelibrary.wiley.com/terms-and-conditions) on Wiley Online Library for rules of use; OA archies are governed by the applicable Centwise Commons I

and minimizing the polarization effects in highly charged LCO cathodes.^[13] Such optimization can reduce the restriction on reversible capacity induced by ineffective voltage drop and enable LCO with high specific capacity at a relatively high discharging voltage plateau within an appropriate voltage range, thereby avoiding violent interfacial side reactions at extremely high charging cut-off voltages. Thus, HV-LCO batteries combining high specific energy, high specific power, and improved safety can be achieved.

With the development of advanced characterization techniques that are highly sensitive at smaller scales and operable in situ, researchers have increasingly focused on the cathodeelectrolyte interphase (CEI) and its impact on battery performance, as the complexity of by-products and the morphological diversity of the CEI complicate its analysis.^[14] The presence of a CEI layer on LCO was first proposed by Goodenough et al.[15] Cherkashinin et al. reported that the CEI layer on LCO became unstable and decomposed when the cathode was charged to 4.5 V.[16] Delmas et al. observed more severe oxidation at the interfaces of fully delithiated LCO.[17] Interfacial side reactions can promote dissolution of transition-metal ions from the cathode, which in turn alters the interfacial chemistry at both electrodes.[18,19] Li et al. used X-ray photoelectron spectroscopy (XPS) to detect the dynamic evolution of the CEI on LCO cathode cycled in a wide potential range up to 4.6 V.[20] Recent studies have emphasized the role of surface structure and electrolyte composition in constructing stable CEI for HV-LCO.[21-23] These results indicate that establishing a stable CEI is critical for achieving excellent interfacial and surficial Li+ kinetics, thereby enabling both high energy density and high power density in batteries. However, relatively few studies have specifically addressed CEI modification for HV-LCO through electrolyte engineering.

Recently, cyclotetrasiloxane compounds have attracted significant attention owing to their dual functionality as precursors for silicon oxycarbide materials and as building blocks for polysiloxane synthesis.^[24–26] The unique ring-opening polymerization characteristics of cyclotetrasiloxanes provide a versatile strategy for constructing polysiloxane-based solid-state electrolytes and polymer-enhanced solid-electrolyte interphase (SEI) layers on the anode, both of which offer high ionic conductivity. [27-30] Furthermore, the diverse functional groups attached to Si atoms in cyclotetrasiloxanes enable the formation of 3D crosslinked networks with other organic molecules. When combined with their inherent ring-opening polymerization reactivity, this versatility yields a wide range of reaction products with tunable properties. Thus, incorporating cyclotetrasiloxane-based additives into electrolytes represents a promising strategy for engineering unique Si-containing CEI structures with tailored characteristics.

introduces This study the newly emerging containing additive, 2,4,6,8-tetramethyl-2,4,6,8organic tetravinylcyclotetrasiloxane (V4D4), into an ethylene carbonate (EC)-based electrolyte with the assistance of fluoroethylene carbonate (FEC) to enhance interfacial depolarization and reconstruct stable interface chemistry on highly delithiated LCO cathodes, enabling high energy and power densities in batteries. Systematic electrochemical measurements are conducted to elucidate the effects of the additives on interfacial electrochemical behavior and their contributions to enhancing battery performance. The underlying depolarization mechanisms are further investigated by combining theoretical calculations and complementary in situ spectroscopic characterization techniques. The strong chelating capability of V4D4 with the surface lattice oxygen of LCO, combined with its HF-scavenging functionality, significantly enhances surficial structural stability and interfacial Li⁺ transport kinetics during the initial charging process, enabling high-capacity delivery of over 220 mA h $\rm g^{-1}$ at 100 mA $\rm g^{-1}$ under an appropriate cut-off voltage of 4.55 V_{II}, with a markedly enhanced O3-H1-3 phase transition in LCO, thereby demonstrating its depolarization effect. Furthermore, the synergy between V4D4 and FEC facilitates the formation of a chemomechanically stable, homogeneous, and fast Li+-conductive CEI enriched with LiF and organosilicon compounds during long-term cycling, thereby ensuring interfacial compatibility and preserving the surface structural integrity of the HV-LCO cathode. This improvement leads to excellent cycle stability and structural reversibility, with a capacity retention of 97% after 200 cycles at high capacity output.

2. Results and Discussion

2.1. V4D4-Modified Electrolyte Enabling HV-LCO Cathode

As aforementioned, the O3CH1-3/O1 phase transition in LCO cathode material at a high charging cut-off voltage is an unavoidable stage in the pursuit of high-capacity delivery and high energy density. However, the concomitant, severe and unmanageable irreversible structural phase transition has led most studies to focus on suppressing this phenomenon, often at the cost of retarding Li de-intercalation kinetics and increasing voltage hysteresis, rather than enhancing its reversibility, which in turn significantly limits the capacity release of LCO at high voltages.

In this study, the effects of V4D4 additive in a common electrolyte on the electrochemical performance of HV-LCO were investigated using various electrochemical measurement techniques. The voltage curves of 4.55 $V_{\rm Li}$ LCO half-cells prepared with different additive formulations after the initial activation process are compared in Figure 1a. The LCO cathode cycled in an additive-free (denoted as BASE hereinafter) electrolyte or in an electrolyte with 5.0 wt.% FEC additive (denoted as FEC hereinafter) exhibited almost the same initial discharge capacity of \approx 186.0 mA h g⁻¹ at a current density of 0.5C (1C = 200 mA g⁻¹). These results were consistent with those in previously reported literature, [9] indicating that the introduction of a small quantity of FEC additive exhibited minimal influence on capacity release. However, electrolytes containing the V4D4 additive evidently increased the discharge capacity of the LCO cathodes with reducing voltage hysteresis, suggesting improved Li de-intercalation kinetics. When 0.5, 0.8, 1.5, 3.0, and 5.0 wt.% V4D4 additives were introduced into the BASE electrolyte, the initial specific discharge capacities of the 4.55 V₁; LCO half-cells increased to \approx 192.5, 200.7, 217.3, 220.4, and 220.3 mA h g⁻¹, respectively. Figure 1b and Figure S1 (Supporting Information) present the effects of V4D4 on the long-term cyclic stability of the 4.55 $V_{\rm Li}$ LCO cathode at a current density of 0.5C. The half-cells with the BASE electrolyte exhibited rapid capacity decay during the initial 30 cycles, dropping to ≈83.1 mA h g⁻¹ after 500 cycles, with a capacity retention of $\approx 45.0\%$. In comparison, the V4D4 additive significantly improved the long-term cycling stability of

15214095, 2025, 44, Downloaded from https://advanced

Lonlinelibrary.wiley.com/doi/10.1002/adma.202504106 by University Town Of Sherzhen, Wiley Online Library on [17/11/2025]. See the Terms and Conditions (https://onlinelibrary.wiley.com/term

and-conditions) on Wiley Online Library for rules of use; OA articles are governed by the applicable Creative Commons

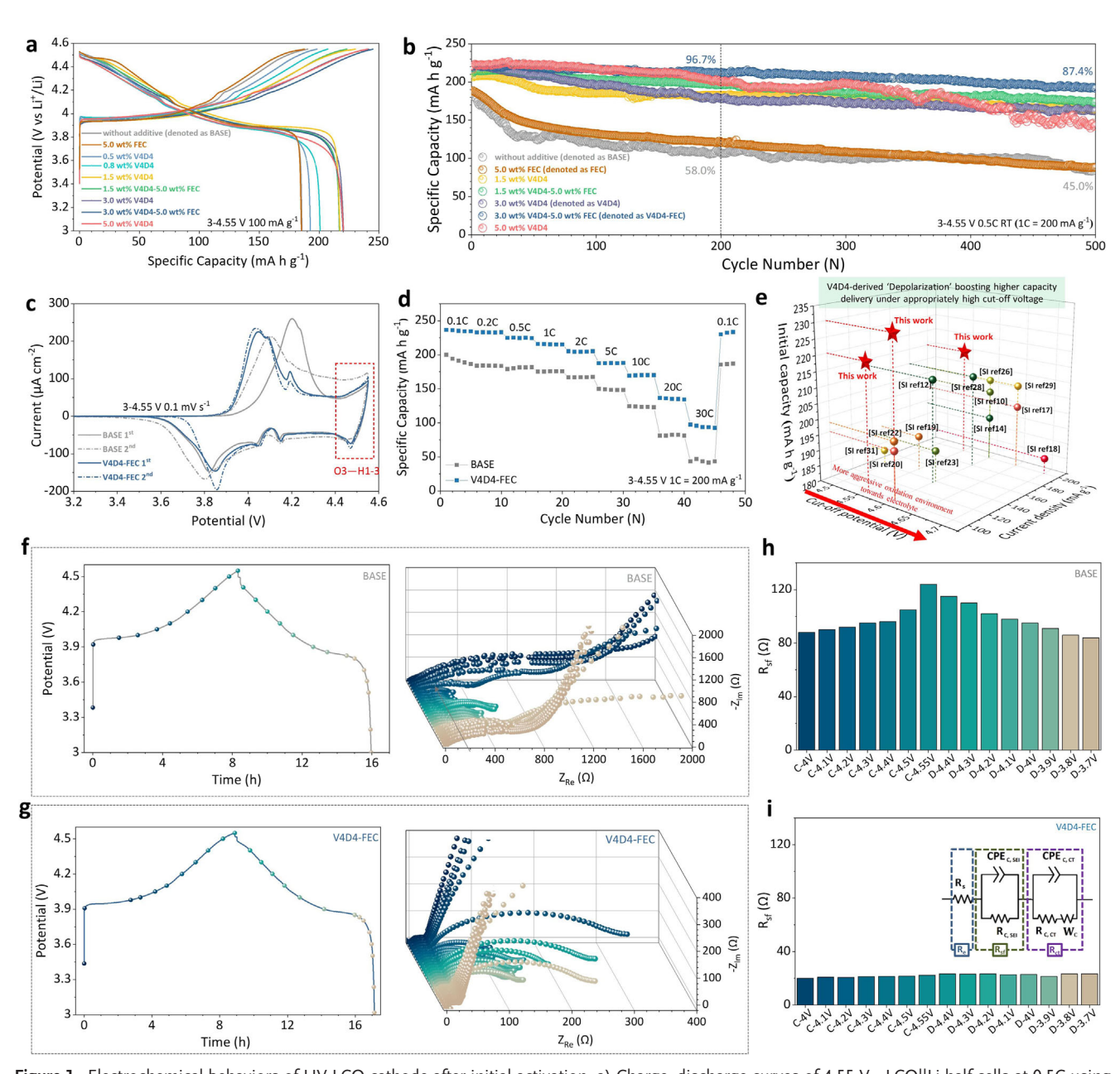


Figure 1. Electrochemical behaviors of HV-LCO cathode after initial activation. a) Charge—discharge curves of 4.55 V_{Li} LCO||Li half cells at 0.5C using different additive formulations. b) Long-term cyclic stability of 4.55 V_{Li} LCO cathode at the current density of 0.5C using different additive formulations. c) CV tests of LCO within a voltage range of 3–4.55 V at a constant voltage scanning of 0.1 mV s⁻¹ in BASE and V4D4-FEC electrolyte. d) Rate performance of 4.55 V_{Li} LCO cathode in BASE and V4D4-FEC electrolyte. e) The summary of the initial specific discharge capacities of LCO cathodes operated at different cut-off voltages and current densities based on various electrolyte systems reported before. The in situ GEIS of LCO in f) BASE and g) V4D4-FEC electrolyte, and the corresponding fitted results of R_{sf} in H) BASE and I) V4D4-FEC electrolyte.

the 4.55 V_{Li} LCO cathode. Specifically, cells with 1.5, 3.0, and 5.0 wt.% V4D4 additives maintained $\approx 79.3\%$, 73.6% and 65.8% of their initial specific discharge capacities after 500 cycles, respectively. Additionally, to further improve the long-term cyclic stability of the 4.55 V_{Li} LCO cathode, FEC was co-added and expected to perform synergistically with V4D4. Cells using electrolytes containing 3.0 wt.% V4D4 and 5.0 wt.% FEC (denoted as V4D4-FEC hereinafter) maintained an initial specific discharge capacity of ≈ 220.0 mA h g⁻¹ and demonstrated the best cyclic

performance with the highest capacity retention of 87.4% after 500 cycles, whereas cells using electrolytes with only 3.0 wt.% V4D4 (denoted as V4D4 hereinafter) exhibited relatively inferior cyclic stability. The LCO||graphite pouch full cell using the V4D4-FEC electrolyte demonstrated outstanding electrochemical cycling performance, highlighting its potential for practical applications (Figure S2, Supporting Information). As shown in Figure S3 (Supporting Information), the V4D4-FEC electrolyte enabled better cyclability of the 4.6 $\rm V_{Li}$ LCO cathode, with the initial

15214095, 2025, 44, Downloaded from https://davanced.onfinitebrary.wiley.com/doi/10.1002/adma.022504106 by University Town Of Shazahen, Wiley Online Library on [17/11/2025]. See the Terms and Conditions (https://onlinelibrary.wiley.com/terms-and-conditions) on Wiley Online Library for rules of use; OA articles are governed by the applicable Centwive Commons In 17/11/2025.

specific discharge capacity reaching \approx 230.1 mA h g⁻¹. Thus, the introduction of V4D4 effectively increased the specific capacity of HV-LCO, and the synergy between V4D4 and FEC further improved its long-term cyclic stability. Considering specific capacity delivery and cycling stability, the optimal proportions of V4D4 and FEC additives introduced into the BASE electrolyte were 3.0 and 5.0 wt.%, respectively.

Figure S4 (Supporting Information) illustrates the activation process for LCO in the BASE, V4D4, and V4D4-FEC electrolytes during the initial cycles within the voltage range of 3-4.55 V at 0.5C. The capacity and average voltage difference during the activation process exhibited opposite trends following the addition of V4D4, confirming the significant influence of the interfacial chemistry of LCO during the initial cycles. A series of electrochemical measurements were conducted to analyze the electrochemical behavior of the HV-LCO cathode and investigate the effects of the V4D4 additive on specific capacity delivery. The galvanostatic intermittent titration technique (GITT) was adopted to analyze differences in Li+ diffusion kinetics during the charge/discharge processes of LCO cathodes cycled in BASE and V4D4-FEC electrolytes, as illustrated in Figure S5 (Supporting Information). The average diffusion coefficients (D_{Ij+}) during charging and discharging of the LCO cathode in the BASE electrolyte were $\approx 4.78 \times 10^{-11}$ and $\approx 4.78 \times 10^{-12}$ cm² s⁻¹, respectively, both lower than the corresponding values of $\approx 2.0 \times$ 10^{-10} and $\approx 3.5 \times 10^{-11}$ cm² s⁻¹ observed in the V4D4-FEC electrolyte, indicating that the V4D4 additive promoted Li⁺ diffusion in the LCO cathode during cycling. Cyclic voltammetry (CV) was performed to further analyze the effect of V4D4 on delithiation and lithiation kinetics. As shown in Figure 1c, the V4D4-FEC system exhibited reduced and more stable voltage hysteresis, and the reversible phase transition between O3 and H1-3 was well maintained, suggesting improved surface depolarization and reversibility of the LCO cathode compared to the BASE system, thereby contributing to increased capacity delivery even at 4.55 V_{II}. Additionally, the LCO cathode cycled in the V4D4-FEC electrolyte demonstrated improved rate capability and high-rate cycling stability (Figure 1d; Figure S6, Supporting Information). Hence, the initial specific discharge capacities of LCO cathodes, operating at different charging cut-off voltages and current densities, were systematically summarized and compared across various previously reported electrolyte-modified systems, as shown in Figure 1e and Table S1 (Supporting Information). In this study, the discharge capacity of the $4.55~V_{Li}$ LCO cathode cycled in the V4D4-FEC electrolyte, which exhibited a remarkable depolarization effect, was even higher than that of the previously reported 4.6 or 4.7 V_{Li}-class LCO cathodes at the same current density, demonstrating that the conventional systems suffered from ineffective voltage drops and a more aggressive oxidation environment at the electrolyte interface that ultimately limited the actual energy release.

To analyze and precisely quantify the enhancement of Li⁺ transport kinetics induced by V4D4 on LCO cathode interfaces, in situ galvanostatic electrochemical impedance spectroscopy (GEIS) was adopted using an LCO—Li—Pt three-electrode system (Figure S7, Supporting Information), which effectively eliminated interference from the anode side impedance signal, as shown in Figure 1f,g. Consistent with previous research, the EIS curves correlated with the state of charge (SOC) of the LCO cath-

ode and were fitted using an equivalent circuit model to extract parameters such as ohmic resistance (Re), surface film resistance (R_{cf}), and the charge transfer resistance (R_{cf}), as illustrated in Figure 1h,i and Figure S8 (Supporting Information).[31-33] The R_{sf}, which corresponded to Li⁺ diffusion through the CEI film on the LCO particle surface, remained highly stable and exhibited lower values in the V4D4-FEC electrolyte compared to those in the BASE electrolyte throughout the charging and discharging process (Figure 1h,i). Thus, the V4D4-FEC additive participated in reconstructing the interface films, resulting in enhanced chemomechanical stability. Denser and more Li+conductive films facilitated improved Li+ diffusion kinetics and offered better protection for the LCO particles, thereby improving battery performance. Moreover, the R_{ct} values increased during the initial cycle in the BASE electrolyte (Figure S8, Supporting Information), indicating poor compatibility between the CEI layers and LCO cathode surfaces, leading to damage of the surface structure and negatively impacting Li⁺ transfer. Conversely, the consistently lower and more stable $R_{\rm ct}$ values observed in the V4D4-FEC electrolyte demonstrated that the interface and surface region of the LCO cathode remained stable with better Li+ transfer kinetics during cycling. Further, the distribution of relaxation time (DRT) curves was extracted from the GEIS data using Fourier transform analysis, as shown in Figure S9 (Supporting Information). The peak observed at the relaxation time (τ) between 0.01 and 0.1 s corresponded specifically to the charge transfer process at the surface of the LCO cathode, [34] and its shift toward higher τ represented the sluggish charge transfer kinetics. In the BASE electrolyte system, the DRT peaks were primarily distributed ≈0.1 s, whereas in the V4D4-FEC system, they appeared near 0.025 s. This difference was notable because it aligned with the R_{ct} fitting results, demonstrating faster Li⁺ transfer kinetics in the V4D4-FEC system.

2.2. V4D4-Induced Depolarization Mechanism Increasing the Initial Capacity Delivery

To determine the modification mechanism behinds, a comprehensive analysis of the intrinsic characteristics of the V4D4-modified electrolyte and the extended electrochemical behavior of the V4D4 additive at the LCO cathode-electrolyte interface after the initial activation was performed.

First, Fourier transform infrared (FTIR) spectroscopy was conducted to evaluate the effects of the additives on the solvation structure of the BASE electrolyte. The results in Figure \$10a (Supporting Information) revealed that the introduction of FEC and V4D4 exhibited minimal effects on the Li+-solvent interactions. Notably, the infrared absorption peaks generated by P-F bond stretching vibration near 840 cm⁻¹ in Figure S10b (Supporting Information) exhibited a redshift after the addition of V4D4, indicating suppression of LiPF₆ (786 cm⁻¹) hydrolysis owing to the reduction in PF₅ (896 cm⁻¹) and PF₃O (909 cm⁻¹) species, which reduced the etching effect of HF on the electrode materials.^[35] The thermostability of the modified electrolyte was tested using liquid nuclear magnetic resonance (NMR). A comparison of the ¹⁹F NMR spectra of BASE, V4D4, and V4D4-FEC electrolyte after storage at 45 °C for a week is shown in Figure S11 (Supporting Information). The HF peak at \approx -156 ppm,

ununu advimat de

15214095, 2025, 44, Downloaded from https://advanced.onlinelibrary.wiley.com/doi/10.1002/adma.202504106 by University Town Of Stenzhen, Wiley Online Library on [17/11/2025]. See the Terms and Conditions (https://onlinelibrary.wiley.com/term

and-conditions) on Wiley Online Library for rules of use; OA articles are governed by the applicable Creative Commons

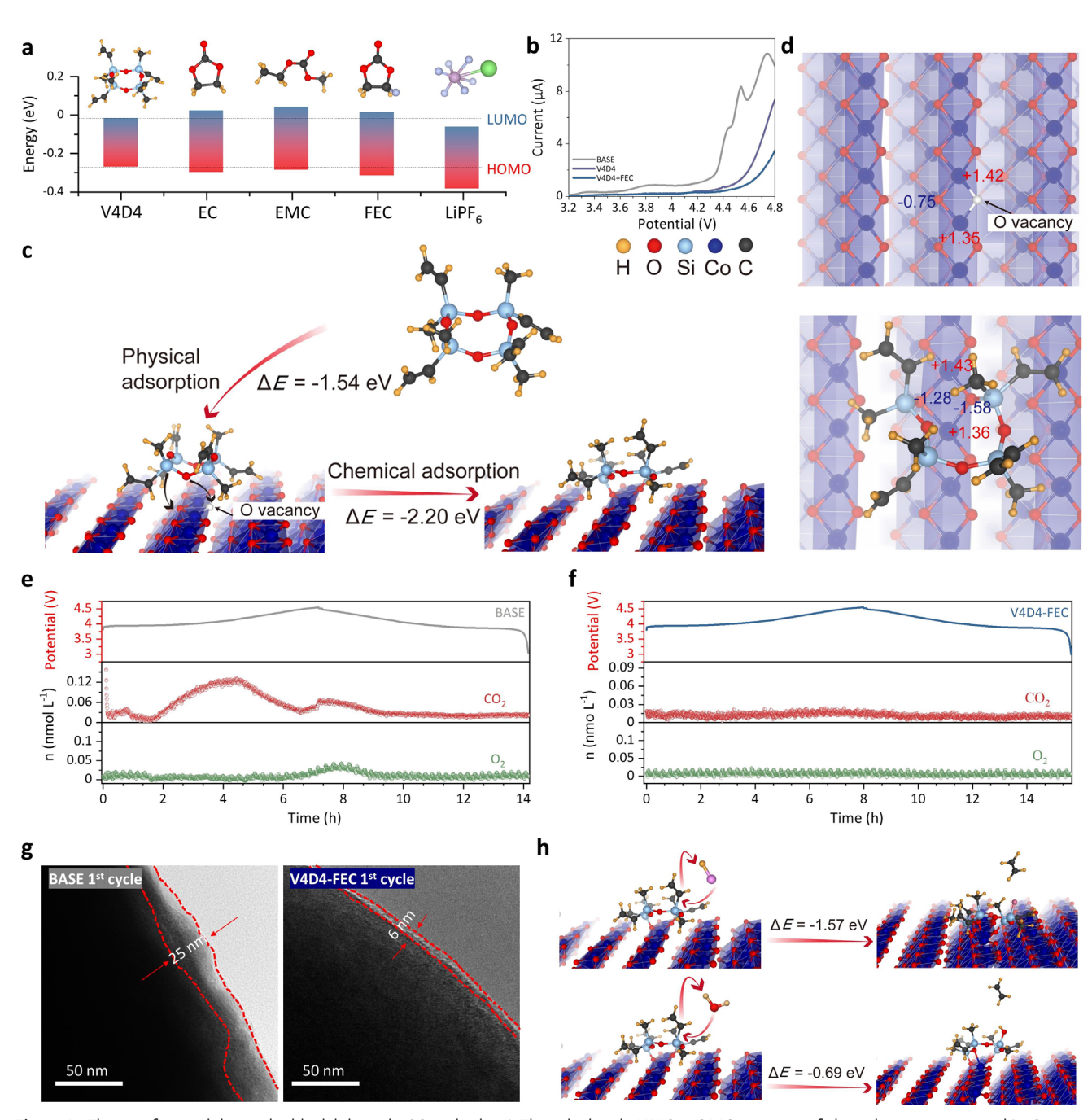


Figure 2. The interface stability on highly-delithiated LCO cathode. a) The calculated LUMO-HOMO energies of electrolyte components. b) LSV measurements of BASE, V4D4, and V4D4-FEC electrolyte on the stainless steel with a scanning rate of 0.1 mV s $^{-1}$. c) The simulation of the electrochemical behaviors of V4D4 additive on the surface of highly-delithiated LCO cathode. d) Bader charge calculations on the surface of highly-delithiated LCO cathode before and after the adsorption of V4D4 oxidation intermediate. In situ DEMS tests for LCO cathode cycled in e) BASE and f) V4D4-FEC electrolyte. g) Cryo-TEM images of CEI on the LCO in different electrolyte after initial activation. h) Calculated reaction energy barrier (\triangle E) for HF/H₂O-Scavenging by absorbed V4D4 oxidation intermediate on the surface.

caused by side reactions of LiPF₆ or FEC, could not be detected, while a new peak at \approx -139 ppm appeared, which originated from the HF/H₂O scavenging by the V4D4 additive to form Si—F species. Therefore, the high-temperature electrochemical cycling performance was significantly improved by the addition of V4D4 (Figure S12, Supporting Information).

The lowest unoccupied molecular orbital (LUMO) and highest occupied molecular orbital (HOMO) energies of the electrolyte components were calculated. A comparison is presented in Table S2 (Supporting Information) and Figure 2a. The V4D4 molecule exhibited the highest HOMO energy, suggesting its preferential oxidation reactivity for reconstructing the initial interface films,

www.advancedsciencenews.com

ADVANCED MATERIALS

www.advmat.de

15214095, 2025, 44, Downloaded from https://davanced.onfinitebrary.wiley.com/doi/10.1002/adma.022504106 by University Town Of Shazahen, Wiley Online Library on [17/11/2025]. See the Terms and Conditions (https://onlinelibrary.wiley.com/terms-and-conditions) on Wiley Online Library for rules of use; OA articles are governed by the applicable Centwive Commons In 17/11/2025.

potentially influencing the subsequent electrochemical decomposition of the bulk electrolyte. The relatively low HOMO and LUMO energies of FEC reflected its dual-functional potential. which enhanced antioxidation stability at the cathode interface and passivated the anode interface. The oxidation resistance of the bulk electrolyte, influenced by V4D4 addition, was further verified by linear sweep voltammetry (LSV) measurements using the Fe-Li-Pt three-electrode system (Figure \$4, Supporting Information). As shown in Figure 2b, a sharp rise in the oxidation current was observed at ≈4.4 V in the BASE electrolyte, which was significantly suppressed and shifted to higher potentials upon the addition of V4D4, demonstrating that the V4D4 additive effectively inhibited excessive oxidative decomposition of the bulk electrolyte at high voltages. Furthermore, V4D4 exhibited an oxidation peak at ≈3.8 V (Figure \$13, Supporting Information), which was consistent with the results of the HOMO calculation. Under the synergy of the FEC additive, the antioxidative capability of the electrolyte was further strengthened.

Figure 2c shows the electrochemical behavior of V4D4 on the surface of the highly delithiated LCO cathode through theoretical simulations. First, the V4D4 molecule physically adsorbed onto the surface lattice structure with an adsorption energy of -1.54 eV. Then, its Si-O chemical bond broke to chemically adsorb and repair oxygen vacancies commonly found in highly delithiated LCO cathodes, with a bonding energy of -2.20 eV, thereby stabilizing the surface lattice oxygen. This stabilization was further confirmed by Bader charge calculations in Figure 2d. The oxygen atom in the LCO cathode slab directly coordinated with the V4D4 oxidation intermediate (8-Si-O) and gained \approx 0.53e in charge after the adsorption reaction; however, the charge on the Co atom remained essentially unchanged. The increase in the charge on the surface lattice oxygen atoms was beneficial for restraining their deep participation in capacity release by charge compensation, which effectively passivated the highly oxidative surfaces of LCO when charging to a high cut-off voltage, thereby suppressing severe irreversible surface structure evolution and weakening the oxidation threat to the bulk electrolyte. This phenomenon was confirmed by performing in situ differential electrochemical mass spectrometry (DEMS) (Figure 2e,f). Analytical results revealed no gas production, except for trace CO₂ throughout cycling with the V4D4-FEC electrolyte. Comparatively, the release of surface lattice O in the form of O₂ occurred at the end of charging in the BASE electrolyte, indicating the instability of the surface lattice O of LCO at high voltages. Additionally, the production of abundant CO2 was observed when charging at ≈4.0 V and above 4.45 V, which resulted from the catalytic oxidative decomposition of EC and EMC solvents by lattice oxygen, O^{n-} (0<n<2) on the LCO surface and the released O₂ gas (Figure S14, Supporting Information). [8,39,40] Apart from gas release, the severe decomposition of electrolyte solvents led to the formation of an initially uneven and thick CEI layer on the LCO surface in the BASE electrolyte, compared to the thinner and more uniform CEI formed in the V4D4-FEC electrolyte, as observed by cryogenic transmission electron microscopy (cryo-TEM) images in Figure 2g and Figure S15 (Supporting Information). Furthermore, the reaction energy barrier ($\triangle E$) for the reactions * + $HF \rightarrow *F + C_2H_4$ (1) and * $+H_2O \rightarrow *OH + C_2H_4$ (2) (* denotes the slab added by 8-Si-O with an oxygen vacancy) was analyzed (Figure 2h). The values of $\triangle E$ for reactions (1)

and (2) were -1.57 and -0.69 eV, respectively, indicating that HF and H2O from the electrolyte attacked the Si-C chemical bond of -Si-C₂H₃ in the slab, forming relatively stable Si-F and Si-OH bonds, along with carbon-chain polymers (polymerization of C₂H₄). Meanwhile, V4D4 underwent ring-opening polymerization to form polysiloxanes with improved ionic conductivity, while its vinyl (-CH=CH2) groups enabled additional polymerization pathways, which facilitated the construction of a robust and functional CEI structure. [29,30] The decomposition pathways of V4D4 during the electrochemical activation are summarized in Figure S16 (Supporting Information).[27,41] The V4D4 additive effectively stabilized the surface lattice O of LCO during the charging process and in situ constructed a beneficial and ultra-thin CEI layer in the process, which substantially improved the interface and surface Li⁺ transport kinetics of LCO and led to depolarization effects. The excellent low-temperature (-20 °C) cyclic performance of the LCO cathode in V4D4-FEC electrolyte further confirmed the optimized Li⁺ transport kinetics in the CEI layer (Figure \$17, Supporting Information).

Furthermore, comprehensive in situ spectroscopic characterization was performed to confirm the initial surface structural stability of the LCO cathode cycled with the V4D4 additive. In situ X-ray diffraction (XRD) measurements were conducted to analyze the evolution of long-range ordered structures during the initial charging and discharging processes based on different electrolyte systems. As shown in **Figure 3**a,b, an association analysis of the (003) and (101) peak evolution of the LCO cathode material was performed. Notably, electrolyte-induced differences at the interface and surface of the LCO cathode exhibited a significant impact on the phase transition process, specifically in the highly delithiated state. [42,43] At a cut-off voltage of 4.55 V_{Ii}, LCO exhibited a significant H1-3 phase transition in the V4D4-FEC electrolyte, corresponding to the Li_{0.2}CoO₂ structure, as calculated using the constant-current charging time. In the BASE system, the H1-3 phase was non-existent, corresponding to the Li_{0.24}CoO₂ structure. The results indicated that the V4D4-FEC electrolyte operation enabled improved Li⁺ transport kinetics and a more reversible capacity for LCO particles in the same cut-off voltage range. Thus, in the BASE electrolyte, gradual surface structure degradation served as the main cause of structural damage to the highly delithiated LCO cathode rather than the O3 to H1-3 phase transition process.[44] Hence, in situ shellisolated nanoparticle enhanced Raman spectroscopy (SHINERS) was used to examine the changes in the surface phase structure. As shown in Figure 3c,d, the Raman peaks located at 485 and 595 cm⁻¹ corresponded to O—Co—O bending vibration (E_a) and Co–O tensile vibration (A_{1g}) modes of the layered LCO cathode, respectively. When charging was performed up to 4.1 V_{Li} for the BASE system, the two peaks significantly weakened and gradually disappeared, recovering until discharging to 3.9 V₁. The phenomenon was attributed to the unstable interfaces in the BASE electrolyte and corresponded to constant changes in R_{of} during cycling for in situ GEIS, thereby affecting the enhancement effect of the Raman signal. Meanwhile, when charging above 4.55 V_{Li} , a new Raman peak appeared at 680 cm $^{-1}$, which was identified as the generation of an irreversible Co₃O₄/CoO phase on the surface, responsible for increased surface polarization.^[45,46] For the V4D4-FEC system, the Raman signal peaks of Eg and A_{1g} existed throughout cycling, the strength of which weakened only

15214095, 2025, 44, Downloaded from https://advanced

l.onlinelibrary.wiley.com/doi/10.1002/adma.202504106 by University Town Of Shenzhen, Wiley Online Library on [17/11/2025]. See the Terms

on Wiley Online Library for rules of use; OA articles are governed by the applicable Creative Commons

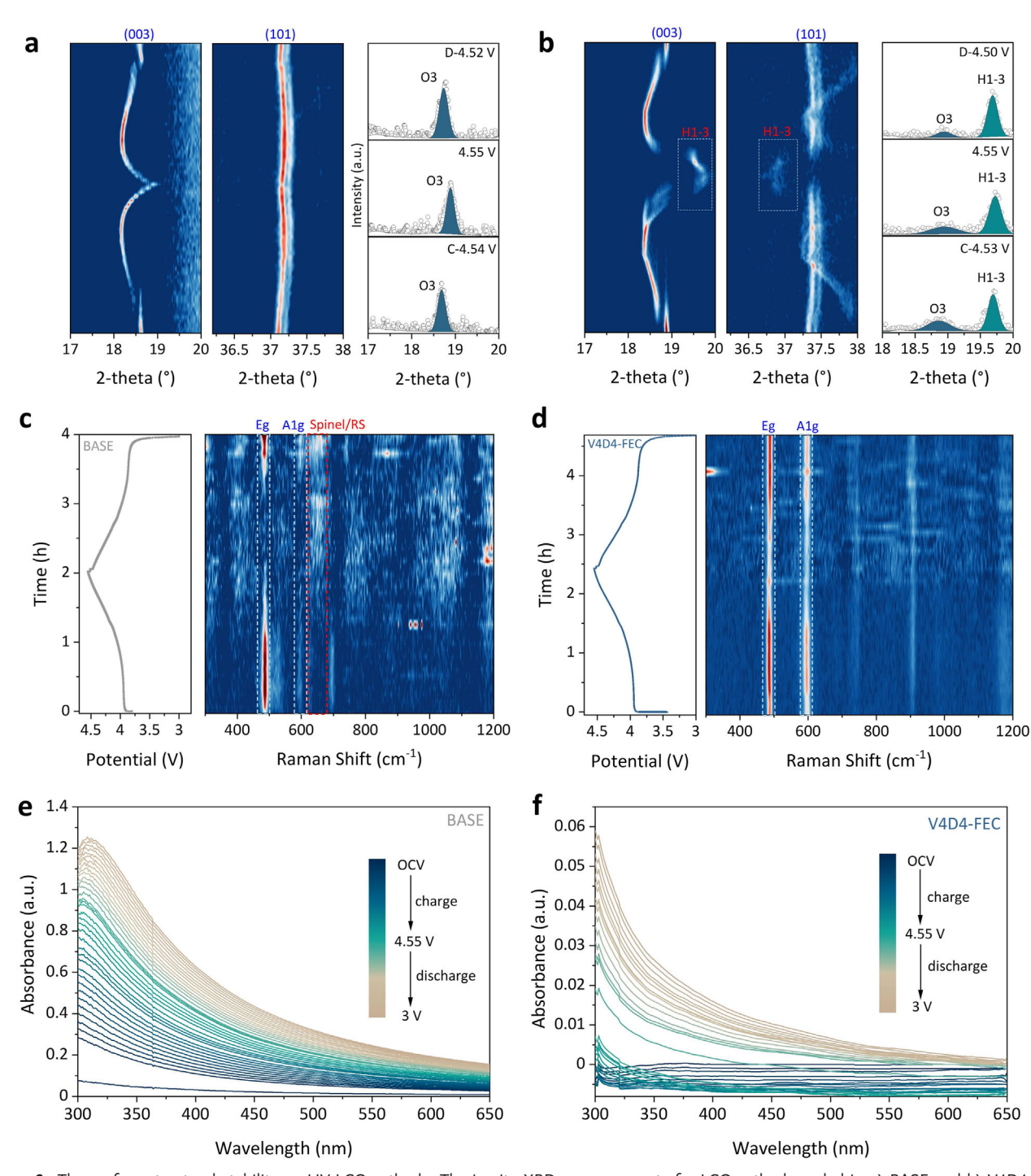


Figure 3. The surface structural stability on HV-LCO cathode. The in situ XRD measurements for LCO cathode cycled in a) BASE and b) V4D4-FEC electrolyte. The in situ SHINERS tests for LCO cathode cycled in c) BASE and d) V4D4-FEC electrolyte. The in situ UV tests for LCO cathode cycled in e) BASE and f) V4D4-FEC electrolyte.

slightly in the high-voltage range. In situ ultraviolet spectroscopy (UVs) was performed to further investigate the dissolution of low-valence Co during the initial cycling process (Figure 3e,f). In the BASE electrolyte, the loss of lattice O in the LCO caused surface TM dissolution and a layered-to-spinel/rock-salt phase transition, while the corrosion of HF led to TM dissolution, both resulting

in capacity loss. In Figure 3e, the UV absorption peak representing Co dissolution into the electrolyte was observed at the 4.0 $\rm V_{Li}$ charging platform. The peak strength gradually increased with cycling, suggesting severe surface degradation. In the V4D4-FEC electrolyte, the intensity of UV absorption was two orders of magnitude lower than that in the BASE electrolyte, even charging

www.advancedsciencenews.com



www.advmat.de

15214095, 2025, 44, Downloaded from https://davanced.onfinitebrary.wiley.com/doi/10.1002/adma.022504106 by University Town Of Shazahen, Wiley Online Library on [17/11/2025]. See the Terms and Conditions (https://onlinelibrary.wiley.com/terms-and-conditions) on Wiley Online Library for rules of use; OA articles are governed by the applicable Centwive Commons In 17/11/2025.

to over 4.4 $V_{\rm Li}$, indicating significant inhibition of Co dissolution and a more stable layered structure of LCO. Therefore, by combining the ultrastable surface lattice O, stabilized and thin CEI layer, and well-maintained surface layered structure in the V4D4-FEC electrolyte, the LCO cathode achieved faster Li⁺ transport kinetics and lower charging/discharging polarization voltage, demonstrating its excellent rate capability and reversible capacity release even at 4.55 $V_{\rm Li}$, which constituted the main content of the proposed depolarization mechanism.

2.3. V4D4-Dominant Surfaces and Interfaces Realizing HV-LCO Cathode for Long-Term Cycles

A higher capacity poses serious challenges to the long-term cyclic stability of structures from outside in, particularly in HV-LCO cathodes.^[47] Hence, identifying the origin of V4D4-dominant stable surfaces and interfaces for long-term cycling is essential. Figure \$18 (Supporting Information) and Figure 4a,b compare the voltage curves and associated dQ/dV curves for the 300 cycles of the LCO||Li cells using BASE and V4D4-FEC electrolytes at a current density of 0.5C in the voltage range of 3–4.55 $V_{\rm Li}$. Similar to the CV curves, the redox peaks in the high-voltage region above 4.4 V_I; corresponded to the O3—H1-3 phase transition. [9] Consistent with the results from in situ XRD analysis, a more obvious H1-3 phase was observed in the V4D4-FEC electrolyte, which was retained even after 300 cycles and demonstrated excellent reversibility. Moreover, the half-peak width and voltage hysteresis of the intensive dQ/dV redox peaks at \approx 3.9 V₁; revealed slight changes throughout 300 cycles, indicating the well-maintained interface and surface structure with fast Li⁺ kinetics. Conversely, the H1-3 phase barely existed in the BASE electrolyte at the beginning and completely disappeared as early cycling progressed. Additionally, the broader O3/O3-II phase transition peaks at ≈3.95 V₁, rapidly decreased in peak intensity with increased voltage hysteresis within 30 cycles, indicating serious damage to the surface and interfacial structure in the BASE electrolyte with progressively increasing polarization. Therefore, to elucidate the degradation in the BASE electrolyte and the improved stability in the V4D4-FEC electrolyte of high-voltage LCO cathodes, a series of structural and component analyses were performed, focusing on the surfaces and interfaces after 30 cycles.

First, the structural evolution of the HV-LCO cathode surface was characterized using ex situ Raman spectroscopy. As illustrated in Figure 4c, the well-preserved A_{1g} and E_{g} vibration peaks indicated the well-maintained layered structure of the LCO cathode cycled in V4D4-FEC electrolyte, whereas the irreversible Co₃O₄/CoO phase at 680 cm⁻¹ appeared in the BASE electrolyte. Surface degradation was confirmed using spherical aberrationcorrected transmission electron microscope (AC-TEM) and the corresponding fast Fourier transform (FFT) (Figure 4d). For the BASE electrolyte, large areas of spinel (Fd-3m) and rock-salt (Fm-3m) phases were observed on the surface of the LCO cathode, some of which exhibited a rock-salt phase with a thickness of ≈19 nm. [48] Additionally, numerous nanoscale microcracks were observed with a spinel phase distributed around, accompanied by severe lattice structure distortion of the layered phase on the surface region, which were related to the internal stress accumulation of the LCO particles caused by the corrosion of HF,

severe Co dissolution and irreversible phase transformation on the surface. [12] For the V4D4-FEC electrolyte, LCO achieved an almost crack-free and lattice-intact layered surface structure with only a 2–5 nm thick mixed spinel-layered surface. Damage to the particle structure was observed on a larger scale using scanning electron microscopy (SEM), as shown in Figure S19 (Supporting Information). The LCO cycled in the BASE electrolyte generated a large number of cracks with widths of over 400 nm. Moreover, severe Co dissolution and migration from the LCO cathode led to the corrosion of the Li metal anode, as shown in Figure S20 (Supporting Information), which was quantitatively verified (Table S3, Supporting Information) by inductively coupled plasma-optical emission spectrometry (ICP-OES).

Furthermore, electron energy loss spectroscopy (EELS) spectra of the Co-L edge of the cycled LCO cathodes based on AC-TEM were obtained to analyze the distribution of the Co valence from the bulk to the surface, as shown in Figure 4e. For the BASE system, the L₃ peak of Co gradually shifted toward a lower energy from the bulk to the surface, indicating that the partial reduction of Co on the surface of the LCO material led to a decrease in the valence state. Conversely, the valence state of Co on the cycled LCO in the V4D4-FEC electrolyte was highly stable, and remained consistent from the bulk to the surface, suggesting superior structural stability and reversibility. The results were confirmed by comparing the EELS spectra of O—K edge of the cycled LCO cathodes. In the BASE electrolyte, the diminished O pre-peaks in the LCO surface region corresponded to the occurrence of the Co₃O₄/CoO phase, whereas in the V4D4-FEC electrolyte, the O-K edge peaks retained a layered phase character. Hard X-ray absorption spectroscopy (XAS) was performed to examine the changes in the Co valence state and the local coordination environment of the LCO material after cycling in different electrolytes. Figure 4f shows the FTextended X-ray absorption fine structure (EXAFX) spectral results for the Co-K edge of the LCO cathodes cycled in different electrolytes after 30 cycles. The peaks at 1.5 and 2.5 Å in the R-space corresponded to the Co-O and Co-Co/Li bonds of LCO, respectively. The Artemis software was used to fit the measured data in the range of 1-3 Å. The coordination numbers of cycled Co-O in BASE and V4D4-FEC electrolytes were 5.81 and 5.96, respectively. Considering that Co was surrounded by six O atoms with a coordination number of 6 in the layered structure of the LCO material, while there were 4 in the Co₃O₄ spinel structure, the lower coordination number of Co-O in the BASE system indicated that more Co₃O₄ spinel phases were generated in the cycled LCO material, which was consistent with the results drawn by Raman and AC-TEM. Figure 4g shows the X-ray absorption near edge structure (XANES) spectra of the Co-K edges of LCO cathodes cycled in different electrolytes after 30 cycles. Compared with the V4D4-FEC electrolyte, the Co absorption edge of the cycled LCO cathode in the BASE electrolyte shifted toward a lower energy, suggesting that more low-valence Co²⁺ was involved when referencing the standard spectra of CoO and Co2O3. The average valence states of Co after cycling with BASE and V4D4-FEC electrolytes were 2.86 and 2.95, respectively. Thus, the V4D4 additive effectively inhibited the reduction of Co during cycling, preventing excessive low-valence Co dissolution, as mentioned in in situ UVs and ICP-OES.

1521 4095, 2025, 44, Downloaded from https://advanced.onlinelibrary.wiley.com/doi/10.1002/adma.202504106 by University Town Of Shenzhen, Wiley Online Library on [17/11/2025]. See the Terms

conditions) on Wiley Online Library for rules of use; OA articles are governed by the applicable Creative Common

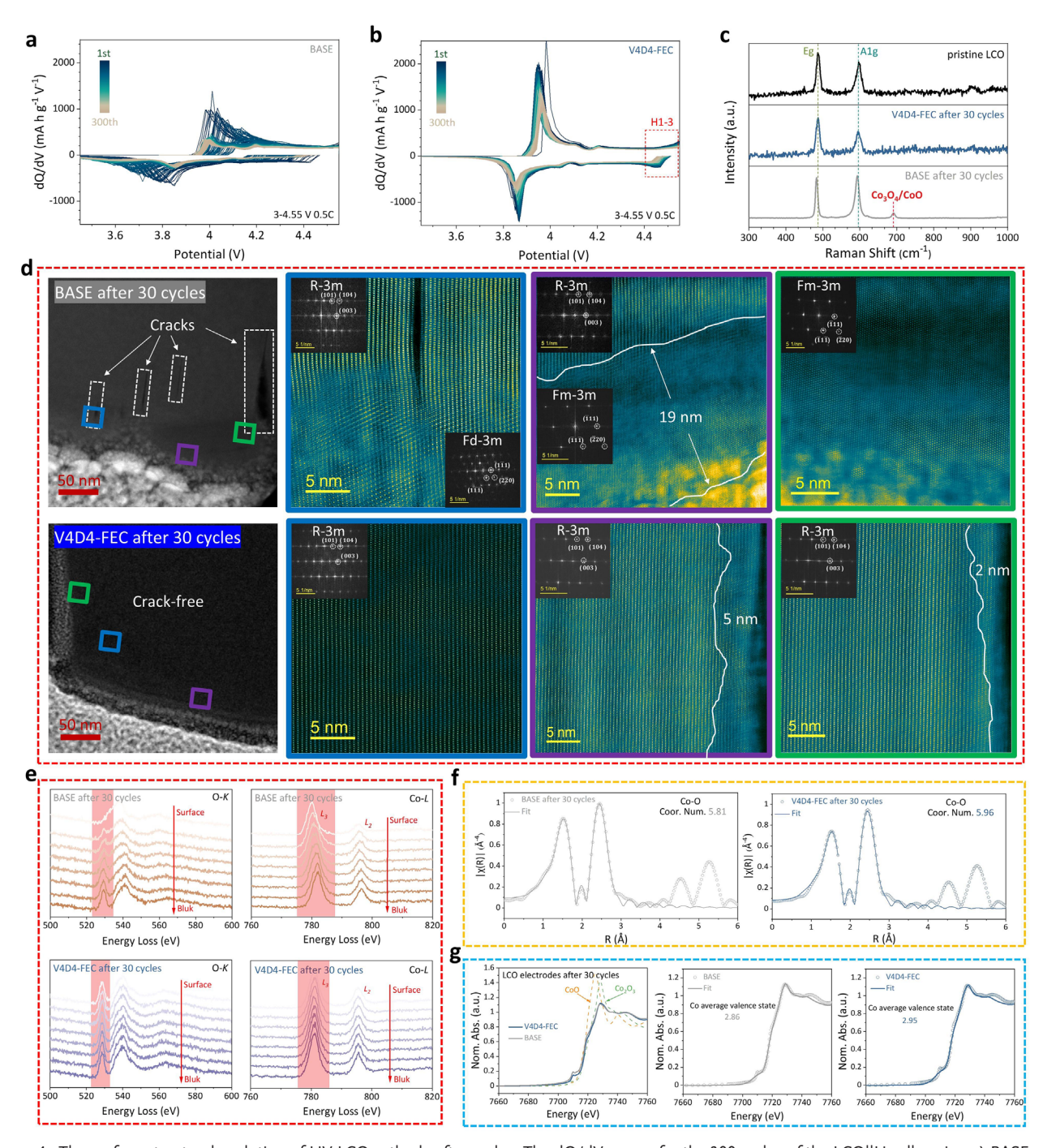


Figure 4. The surface structural evolution of HV-LCO cathode after cycles. The dQ/dV curves for the 300 cycles of the LCO||Li cells using a) BASE and b) V4D4-FEC electrolytes at the current density of 0.5C in the voltage range of 3–4.55 V_{Li} . c) The ex situ Raman spectroscopy of LCO cathode cycled in different electrolyte after 30 cycles. d) The AC-TEM and corresponding FFT of LCO cathode cycled in different electrolyte after 30 cycles, and the e) EELS spectra of Co—L edge of the cycled LCO cathodes from the bulk to the surface region. f) The EXAFX and g) XANES spectral results of Co—K edge of the LCO cathodes cycled in different electrolytes after 30 cycles.

The interfacial evolution of the HV-LCO cathode served as another critical factor influencing its long-term cyclic stability, which contributed to its surface structural stability. A comprehensive characterization was conducted to examine the structures and components of the CEI layers formed in different electrolytes. The cyro-TEM images (**Figure 5a**) revealed the uneven

and thick CEI layers formed in the BASE electrolyte after 30 cycles, suggesting instability and continuous decomposition of the bulk electrolyte. However, the CEI layers formed in the V4D4-FEC electrolyte resulted in a uniform, dense, and thin structure, the thickness of which was slightly increased to 10 nm compared with the initial cycle (Figure 2g). As shown in Figure S21

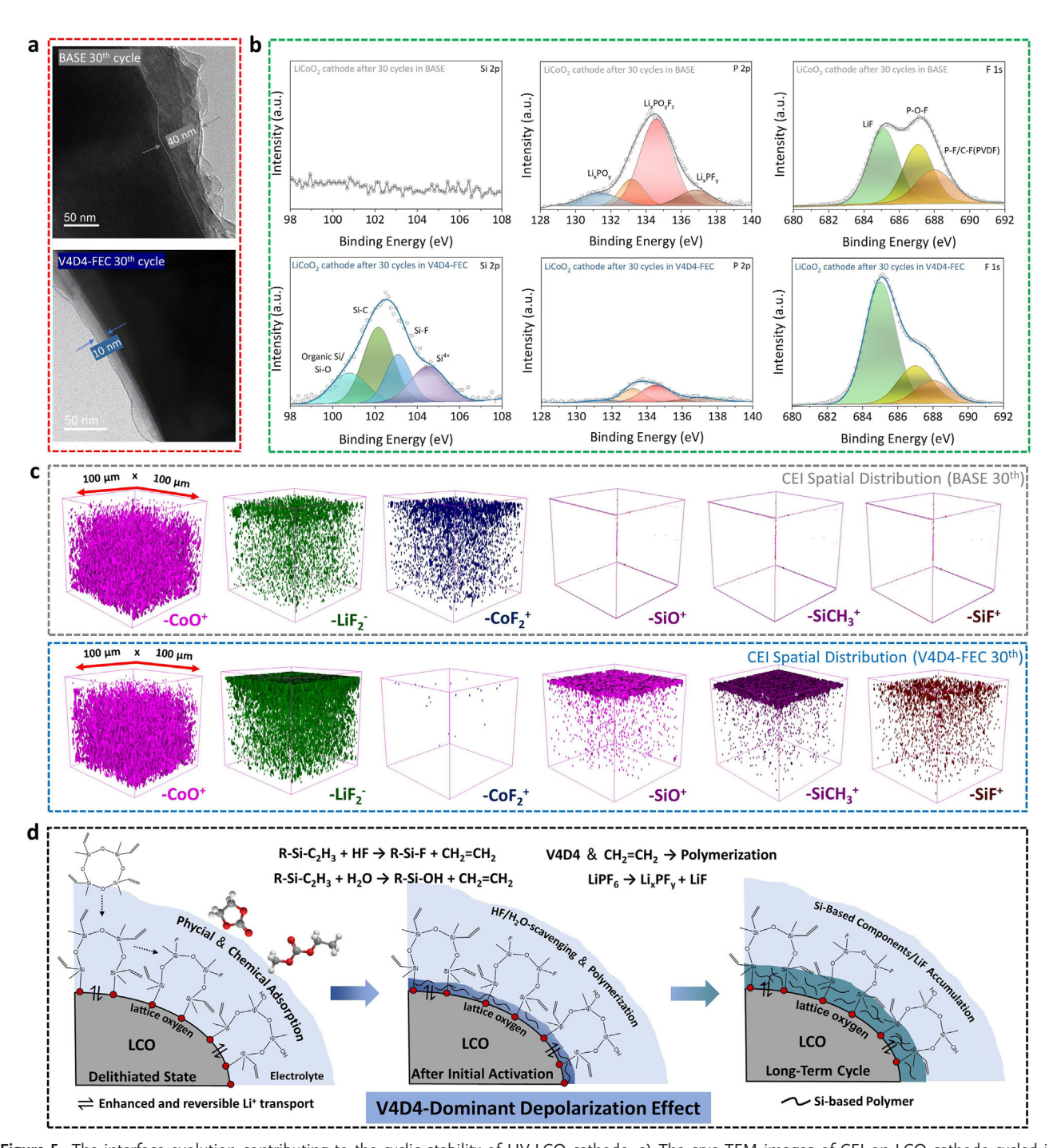


Figure 5. The interface evolution contributing to the cyclic stability of HV-LCO cathode. a) The cryo-TEM images of CEI on LCO cathode cycled in different electrolyte after 30 cycles. b) The XPS spectra and c) 3D reconstruction of time-of-flight secondary ion mass spectroscopy for the distribution of components in CEI on the LCO cathode cycled in different electrolyte after 30 cycles. d) The schematic diagram of the mechanism of V4D4-FEC synergetic additive to achieve depolarization effects and cyclic stability of HV-LCO cathode.

(Supporting Information), the uniformly distributed detected Si and F element signals in the energy-dispersive spectroscopy (EDS) images preliminarily demonstrated the participation of additives in the formation of CEI layers on the LCO cathode surfaces cycled in the V4D4-FEC electrolyte. X-ray photoelectron spectroscopy (XPS) was performed on the cycled LCO electrodes

using different electrolytes to further analyze the effects of the additives introduced on the chemical compositions of the interfacial films. As shown in Figure 5b and Figure S22 (Supporting Information), the Si 2p spectra, V4D4 additive influenced the construction of the interface films by generating organic Si compounds. Additionally, the existence of Si—O and Si—F species verifies the

for rules of use; OA articles are governed by the applicable Crea

1521 4095, 2025, 44, Downloaded from https://advanced.onlinelibrary.wiley.com/doi/10.1002/adma.202504 106 by University Town Of Shenzhen, Wiley Online Library on [17/11/2025]. See the Terms and Conditions (https://onlinelibrary.wiley.com/terms

and-conditions) on Wiley Online Library for rules of use; OA articles are governed by the applicable Creative Commons

hypothesis that the oxidized intermediates of the V4D4 additive help stabilize the surface lattice oxygen and scavenge the detrimental by-products of $\rm H_2O$ and HF. As for the P 2p spectra, the peaks located in the range of 132–136 eV can be identified as the series of hydrolysates of the LiPF $_6$ salt, the contents of which obviously decreased in the presence of the V4D4 additive, confirming the elimination of $\rm H_2O$. Thus, the decomposition of the LiPF $_6$ salt on the surface of LCO can produce a LiF component rather than a $\rm Li_x PO_y F_z$ species, as confirmed by the F 1s spectra. This shows that LiF is enriched in the interface films of the LCO cathode, which can improve the chemomechanical stability during long-term cycling. The introduction of V4D4 and FEC co-additives can also enhance the interfacial stability of the Li anode, constructing a stable SEI layer enriched with LiF and silicon-containing compounds (Figure S23, Supporting Information).

As shown in Figure 5c, multilayer ion analysis and 3D reconstruction of time-of-flight secondary ion mass spectra (TOF-SIMS) were used to observe the spatial distribution of the components in the CEI layers. LiF was densely distributed in the CEI layers formed in the V4D4-FEC electrolyte. Moreover, compact Si-C, Si-O, and Si-F compound compositions were observed in the superficial structure of the CEI layers, demonstrating that the V4D4 additive assisted in the formation of uniform and dense CEI layers rich in organic Si compounds to stabilize the surfaces and interfaces on high-voltage LCO cathodes. Meanwhile, an obvious CoF2 ion fragment signal existed on the LCO surface in the BASE system, which corresponded to cobalt fluoride generated by a more serious corrosion reaction between HF and the LCO material surface. The SiF ion fragment signal detected in the V4D4-FEC system further proved the elimination function of HF. Accordingly, the CEI components of LCO cycled in the BASE and V4D4-FEC electrolytes exhibited significant differences, and further impacted the Li⁺ kinetics across the surface and interface regions. Figure S24 (Supporting Information) compares the EIS curves of the cells with those of the BASE and V4D4-FEC electrolytes after different numbers of cycles, and the fitting results are listed in Table S4 (Supporting Information). For the BASE system, the R_{ct} value sharply increased to 1480 and 2145 Ω after 30 and 100 cycles, respectively, indicating the inferior Li⁺ diffusion kinetics on the LCO surface and large polarization, while the R_{ct} value in the V4D4-FEC system changed slightly, demonstrating the stable surface structure with better Li+ transfer kinetics even after long-term cycles.

The working mechanism of the V4D4-FEC synergetic additive to achieve depolarization effects and the cyclic stability of the HV-LCO cathode is illustrated in Figure 5d. For the BASE electrolyte, the highly oxidative surface of LCO at high voltages can cause constant decomposition of the electrolyte solvents and surface Co/O loss, leading to uneven and loose CEI formation and irreversible layered-to-spinel/rock-salt phase evolution, resulting in a sharp increase in polarization at the interface and surface regions (Figure \$25, Supporting Information). In contrast, in Figure 5d, the preferential oxidation decomposition and atomic-scale interactions of the V4D4 additive on the highly delithiated LCO cathode interface reinforce the surface lattice oxygen to stabilize the layered structure at high voltage and act as scavengers to avoid HF attack. The ring-opening polymerization of V4D4 can generate polysiloxane-based components with high ionic conductivity, thereby further optimizing the CEI layer. As a result, under the synergy of the FEC additive, a thin, uniform, and dense CEI layer dominated by organic Si-containing compounds and LiF is constructed on the LCO, revealing chemomechanically stable and fast Li⁺-conductive properties, which suppress excessive decomposition of electrolyte solvents and further promote the surface structure stability and reversibility of the O3—H1-3 bulk phase transition. The stable surface and interface with the depolarization effect enabled an LCO cathode with high-capacity delivery at 4.55 $\rm V_{li}$.

3. Conclusion

This study achieves a Li+-conductive and stable surface and interface on an HV-LCO cathode using the proposed V4D4-FECsynergetic electrolyte. The preferentially oxidized intermediate of the V4D4 additive acts as both a chelating agent, stabilizing lattice O, and an HF scavenger, preventing severe etching of the highly delithiated LCO surface. This dual functionality leads to the formation of a thin, homogeneous interfacial layer with a pronounced depolarization effect, enabling excellent rate capability and reversible capacity of \approx 220 mA h g⁻¹ for an LCO cathode charged only to $4.55 V_{Li}$. The results are comparable to the capacity achieved at higher charging cut-off voltages of 4.6–4.7 V_{Li} in conventional electrolyte systems, but without additional energy loss or increased safety concerns. During long-term cycling, the synergy between the FEC co-additive and the pivotal V4D4 additive facilitates the formation of a chemo-mechanically stable and Li⁺-conductive interphase enriched with LiF and organic Si compounds. This interphase strengthens the stability and reversibility of the significantly enhanced O3-H1-3 phase transition in the HV-LCO cathode, resulting in a capacity retention of ≈97% after 200 cycles. Overall, based on the interface depolarization mechanism, precise interfacial engineering is achieved though the V4D4-FEC electrolyte design, offering valuable guidelines for developing high-energy-density LCO batteries with excellent performance at appropriate charging cut-off voltages.

Supporting Information

Supporting Information is available from the Wiley Online Library or from the author.

Acknowledgements

G.Z., H.R., and J.Q. contributed equally to this work. This work was financially supported by the National Natural Science Foundation of China (Grant Nos. 22479087 and 52203298), the Natural Science Foundation of Guangdong Province (Grant No. 2024B1515020092), Shenzhen Postdoctoral Research Foundation (Grant No. 04070100125), the International Joint Research Center for Electric Vehicle Power Battery and Materials (Grant No. 2015B01015), the Basic and Applied Basic Research Foundation of Guangdong Province (Grant No. 2021B1515130002), Guangdong Key Laboratory of Design and Calculation of New Energy Materials (Grant No. 2017B030301013), and Shenzhen Key Laboratory of New Energy Resources Genome Preparation and Testing (Grant No. ZDSYS201707281026184).

Conflict of Interest

The authors declare no conflict of interest.

1521 4095, 2025, 44, Downloaded from https://advanced.onlinelibrary.wiley.com/doi/10.1002/adma.202504 106 by University Town Of Shenzhen, Wiley Online Library on [17/11/2025]. See the Terms and Conditions (https://onlinelibrary.wiley.com/terms

and-conditions) on Wiley Online Library for rules of use; OA articles are governed by the applicable Creative Common

Data Availability Statement

The data that support the findings of this study are available from the corresponding author upon reasonable request.

Keywords

cathode-electrolyte interphase, cyclotetrasiloxanes, depolarization, interface chemistry, LiCoO2

Received: February 28, 2025 Revised: August 13, 2025 Published online: August 21, 2025

- [1] K. Mizushima, P. C. Jones, P. J. Wiseman, J. B. Goodenough, *Mater. Res. Bull.* 1980, 15, 783.
- [2] Z. Wang, Z. Wang, W. Peng, H. Guo, X. Li, J. Wang, A. Qi, *Ionics* 2014, 20, 1525.
- [3] J. Zheng, J. Lu, K. Amine, F. Pan, Nano Energy 2017, 33, 497.
- [4] J. Li, C. Lin, M. Weng, Y. Qiu, P. Chen, K. Yang, W. Huang, Y. Hong, J. Li, M. Zhang, C. Dong, W. Zhao, Z. Xu, X. Wang, K. Xu, J. Sun, F. Pan, Nat. Nanotechnol. 2021, 16, 599.
- [5] H. Ren, W. Zhao, H. Yi, Z. Chen, H. Ji, Q. Jun, W. Ding, Z. Li, M. Shang, J. Fang, K. Li, M. Zhang, S. Li, Q. Zhao, F. Pan, Adv. Funct. Mater. 2023, 33, 2302622.
- [6] X. Wang, H. Ren, Y. Du, Z. Li, W. Zhao, H. Ji, H. Yi, Q. Pan, J. Liu, Z. Lou, L. Zhou, F. Pan, Q. Zhao, Nano Energy 2024, 125, 109537.
- [7] A. Van der Ven, M. K. Aydinol, G. Ceder, J. Electrochem. Soc. 1998, 145, 2149.
- [8] B. L. D. Rinkel, D. S. Hall, I. Temprano, C. P. Grey, JACS 2020, 142, 15058.
- [9] X. Yang, M. Lin, G. Zheng, J. Wu, X. Wang, F. Ren, W. Zhang, Y. Liao, W. Zhao, Z. Zhang, N. Xu, W. Yang, Y. Yang, Adv. Funct. Mater. 2020, 30, 2004664.
- [10] W. Ding, H. Ren, Z. Li, M. Shang, Y. Song, W. Zhao, L. Chang, T. Pang, S. Xu, H. Yi, L. Zhou, H. Lin, Q. Zhao, F. Pan, Adv. Energy Mater. 2024, 14. 2303926.
- [11] X. Yang, C. Wang, P. Yan, T. Jiao, J. Hao, Y. Jiang, F. Ren, W. Zhang, J. Zheng, Y. Cheng, X. Wang, W. Yang, J. Zhu, S. Pan, M. Lin, L. Zeng, Z. Gong, J. Li, Y. Yang, Adv. Energy Mater. 2022, 12, 2200197.
- [12] Y. Jiang, C. Qin, P. Yan, M. Sui, J. Mater. Chem. A 2019, 7, 20824.
- [13] S. Xu, X. Tan, W. Ding, W. Ren, Q. Zhao, W. Huang, J. Liu, R. Qi, Y. Zhang, J. Yang, C. Zuo, H. Ji, H. Ren, B. Cao, H. Xue, Z. Gao, H. Yi, W. Zhao, Y. Xiao, Q. Zhao, M. Zhang, F. Pan, *Angew. Chem., Int. Ed.* 2023, 62, 202218595.
- [14] J. Xiao, N. Adelstein, Y. Bi, W. Bian, J. Cabana, C. L. Cobb, Y. Cui, S. J. Dillon, M. M. Doeff, S. M. Islam, K. Leung, M. Li, F. Lin, J. Liu, H. Luo, A. C. Marschilok, Y. S. Meng, Y. Qi, R. Sahore, K. G. Sprenger, R. C. Tenent, M. F. Toney, W. Tong, L. F. Wan, C. Wang, S. E. Weitzner, B. Wu, Y. Xu, Nat. Energy 2024, 9, 1463.
- [15] M. G. S. R. Thomas, P. G. Bruce, J. B. Goodenough, *Solid State Ionics* 1985, 17, 13.
- [16] G. Cherkashinin, K. Nikolowski, H. Ehrenberg, S. Jacke, L. Dimesso, W. Jaegermann, Phys. Chem. Chem. Phys. 2012, 14, 12321.
- [17] L. Dahéron, R. Dedryvère, H. Martinez, M. Ménétrier, C. Denage, C. Delmas, D. Gonbeau, Chem. Mater. 2008, 20, 583.
- [18] K. Wang, L. Xing, K. Xu, H. Zhou, W. Li, ACS Appl. Mater. Interfaces 2019, 11, 31490.

- [19] S. Komaba, N. Kumagai, Y. Kataoka, Electrochim. Acta 2002, 47, 1229.
- [20] J.-N. Zhang, Q. Li, Y. Wang, J. Zheng, X. Yu, H. Li, Energy Storage Mater. 2018, 14, 1.
- [21] H. Ren, G. Zheng, Y. Li, S. Chen, X. Wang, M. Zhang, W. Zhao, H. Yi, W. Huang, J. Fang, T. Liu, L. Yang, M. Liu, Q. Zhao, F. Pan, Energy Environ. Sci. 2024, 17, 7944.
- [22] H. Ren, J. Hu, H. Ji, Y. Huang, W. Zhao, W. Huang, X. Wang, H. Yi, Y. Song, J. Liu, T. Liu, M. Liu, Q. Zhao, F. Pan, Adv. Mater. 2024, 36, 2408875.
- [23] H. Ren, X. Wang, W. Ding, C. Xu, W. Zhao, H. Ji, H. Yi, Z. Zhan, Y. Song, L. Zhou, Q. Zhao, F. Pan, Adv. Funct. Mater. 2025, https://doi.org/10.1002/adfm.202504165.
- [24] R. Bhandavat, G. Singh, J. Phys. Chem. C 2013, 117, 11899.
- [25] N. A. A. Rossi, R. West, Polym. Int. 2009, 58, 267.
- [26] R. Spindler, D. F. Shriver, Macromolecules 1988, 21, 648.
- [27] S. Wang, Y. He, G. Zhang, K. Ma, C. Wang, F. Zhou, Z. Wang, Z. Liu, Z. Lu, X. Huang, Y. Zhang, Adv. Energy Mater. 2024, 14, 2401384.
- [28] X. He, J. Lin, G. Ge, F. Yan, K. Zhu, B. Shen, J. Zhai, J. Power Sources 2023, 555, 232346.
- [29] M. Gruenebaum, M. M. Hiller, S. Jankowski, S. Jeschke, B. Pohl, T. Schuermann, P. Vettikuzha, A.-C. Gentschev, R. Stolina, R. Mueller, H.-D. Wiemhoefer, *Prog. Solid State Chem.* 2014, 42, 85.
- [30] T. Mizumo, M. Nakashima, J. Ohshita, Silicon 2017, 9, 85.
- [31] L. Wang, J. Ma, C. Wang, X. Yu, R. Liu, F. Jiang, X. Sun, A. Du, X. Zhou, G. Cui, Adv. Sci. 2019, 6, 1900355.
- [32] D. Zhao, J. Wang, P. Wang, H. Liu, S. Li, Electrochim. Acta 2020, 337, 135745.
- [33] W. Hu, Y. Peng, Y. Wei, Y. Yang, J. Phys. Chem. C 2023, 127, 4465.
- [34] Y. Lu, C.-Z. Zhao, J.-Q. Huang, Q. Zhang, Joule 2022, 6, 1172.
- [35] Y. Yan, S. Weng, A. Fu, H. Zhang, J. Chen, Q. Zheng, B. Zhang, S. Zhou, H. Yan, C.-W. Wang, Y. Tang, H. Luo, B.-W. Mao, J. Zheng, X. Wang, Y. Qiao, Y. Yang, S.-G. Sun, ACS Energy Lett. 2022, 7, 2677.
- [36] K. Kim, D. Hwang, S. Kim, S. O. Park, H. Cha, Y. S. Lee, J. Cho, S. K. Kwak, N. S. Choi, Adv. Energy Mater. 2020, 10, 2000012.
- [37] S. Wilken, M. Treskow, J. Scheers, P. Johansson, P. Jacobsson, RSC Adv. 2013, 3, 16359.
- [38] N. Dupre, M. Cuisinier, D. Guyomard, Electrochem. Soc. Interface 2011. 20. 61.
- [39] S. Kang, D. Choi, H. Lee, B. Choi, Y. M. Kang, Adv. Mater. 2023, 35, 2211965.
- [40] B. L. D. Rinkel, J. P. Vivek, N. Garcia-Araez, C. P. Grey, Energy Environ. Sci. 2022, 15, 3416.
- [41] W. Hou, Q. Feng, C. Liu, X. Zhang, J. Yue, Q. Tian, S. Wu, Y. Ou, P. Zhou, Y. Xia, Y. Wang, X. Song, H. Zhou, Y. Lu, S. Yan, K. Liu, Adv. Mater. 2025, 37, 2503893.
- [42] Y. Lyu, X. Wu, K. Wang, Z. Feng, T. Cheng, Y. Liu, M. Wang, R. Chen, L. Xu, J. Zhou, Y. Lu, B. Guo, Adv. Energy Mater. 2020, 11, 2000982.
- [43] L. Wang, B. Chen, J. Ma, G. Cui, L. Chen, Chem. Soc. Rev. 2018, 47, 6505.
- [44] J.-N. Zhang, Q. Li, C. Ouyang, X. Yu, M. Ge, X. Huang, E. Hu, C. Ma, S. Li, R. Xiao, W. Yang, Y. Chu, Y. Liu, H. Yu, X.-Q. Yang, X. Huang, L. Chen, H. Li, *Nat. Energy* **2019**, *4*, 594.
- [45] W. M. Seong, K. Yoon, M. H. Lee, S.-K. Jung, K. Kang, Nano Lett. 2018, 19, 29.
- [46] G. Sun, F.-D. Yu, M. Lu, Q. Zhu, Y. Jiang, Y. Mao, J. A. McLeod, J. Maley, J. Wang, J. Zhou, Z. Wang, Nat. Commun. 2022, 13, 6464.
- [47] Y. Wang, C. Xu, X. Tian, S. Wang, Y. Zhao, Chin. J. Struct. Chem. 2023, 42. 100167.
- [48] W. Zhu, J. Zhang, J. Luo, C. Zeng, H. Su, J. Zhang, R. Liu, E. Hu, Y. Liu, W. D. Liu, Y. Chen, W. Hu, Y. Xu, Adv. Mater. 2022, 35, 2208974.